Stem Cell Reports
Report

ISSCR

OPEN ACCESS

Direct Reprogramming of Resident NG2 Glia into Neurons with Properties of Fast-Spiking Parvalbumin-Containing Interneurons

Maria Pereira,[1] Marcella Birtele,[1] Shelby Shrigley,[1] Julio Aguila Benitez,[2] Eva Hedlund,[2] Malin Parmar,[1,3,*] and Daniella Rylander Ottosson[1,3,*]

[1]Department of Experimental Medical Science and Lund Stem Cell Center BMC, Lund University, 22632 Lund, Sweden
[2]Department of Neuroscience, Karolinska Institutet, Retzius v.8, 17177 Stockholm, Sweden
[3]Co-senior author
*Correspondence: malin.parmar@med.lu.se (M.P.), daniella.ottosson@med.lu.se (D.R.O.)
http://dx.doi.org/10.1016/j.stemcr.2017.07.023

SUMMARY

Converting resident glia into functional and subtype-specific neurons *in vivo* by delivering reprogramming genes directly to the brain provides a step forward toward the possibility of treating brain injuries or diseases. To date, it has been possible to obtain GABAergic and glutamatergic neurons via *in vivo* conversion, but the precise phenotype of these cells has not yet been analyzed in detail. Here, we show that neurons reprogrammed using *Ascl1*, *Lmx1a*, and *Nurr1* functionally mature and integrate into existing brain circuitry and that the majority of the reprogrammed neurons have properties of fast-spiking, parvalbumin-containing interneurons. When testing different combinations of genes for neural conversion with a focus on pro-neural genes and dopamine fate determinants, we found that functional neurons can be generated using different gene combinations and in different brain regions and that most of the reprogrammed neurons become interneurons, independently of the combination of reprogramming factors used.

INTRODUCTION

Direct cellular reprogramming provides a route to generate neurons from somatic cells *in vitro* (Vierbuchen et al., 2010) that opens up new possibilities to obtain patient- and disease-specific neurons, and several groups have reported successful reprogramming into functional neurons of distinct subtypes *in vitro* (reviewed in Masserdotti et al., 2016). More recently, it has been shown that non-neural cells can be reprogrammed into functional neurons *in situ* (reviewed in Grealish et al., 2016). Many of the neurons obtained acquire a GABAergic or glutamatergic identity (Grande et al., 2013; Torper et al., 2015), but the exact subtype identity and how fate specification is controlled during *in vivo* conversion remains an important question.

In this study, we performed a time-course analysis of NG2 glia reprogrammed into neurons using *Ascl1*, *Lmx1a*, and *Nurr1* (ALN). We show that *in vivo* reprogrammed neurons functionally mature over time and that their ability to fire action potentials (AP) precedes circuitry integration. We also reprogrammed neurons in the dopamine (DA)-depleted striatum and in the midbrain, and tested different combinations of pro-neural genes and DA fate determinants. In all these conditions, we found only minor differences in the phenotype of the reprogrammed cells. A detailed analysis using electrophysiology, immunohistochemistry, and transcriptional profiling showed that most of the reprogrammed neurons acquire properties of fast-spiking (FS), parvalbumin (PV)+ interneurons (IntNs), a neuronal subtype that plays a highly interesting role in striatal function and with potentially important therapeutic roles.

RESULTS

Gradual Maturation into Functional Neurons

We injected *NG2*-Cre mice with CRE-dependent ALN conversion vectors and a GFP reporter that specifically labels reprogrammed neurons (Torper et al., 2015). To estimate the conversion efficiency, we also injected animals (n = 3) with a Cre-dependent GFP under the ubiquitous chicken beta-actin (cba) promoter rendering all targeted cells GFP+. We found that the vectors efficiently targeted NG2 glia (Figure S1A), and estimated that 66.81% ± 38.38% of targeted cells converted into neurons (Figure S1B).

Reprogrammed neurons were detected by their endogenous GFP expression (Figure 1A). Biocytin neuronal filling of such GFP + neurons revealed mature neuronal morphologies and extensive dendritic trees of the reprogrammed neurons (Figure 1B). Electrophysiological recordings performed on the GFP-expressing neurons 5, 8, or 12 weeks post-injection (w.p.i.). showed that membrane-intrinsic properties gradually matured: Membrane capacitance (Cm) increased (Figure 1C), while the input resistance and the resting-membrane potential (RMP) decreased (Figures 1D and 1E), indicating that the cells acquired more ion channels, increased in size, and gained more elaborate morphology with time. During the same time period, the frequency of spontaneous postsynaptic activity increased, suggesting added postsynaptic connections (Figure 1F).

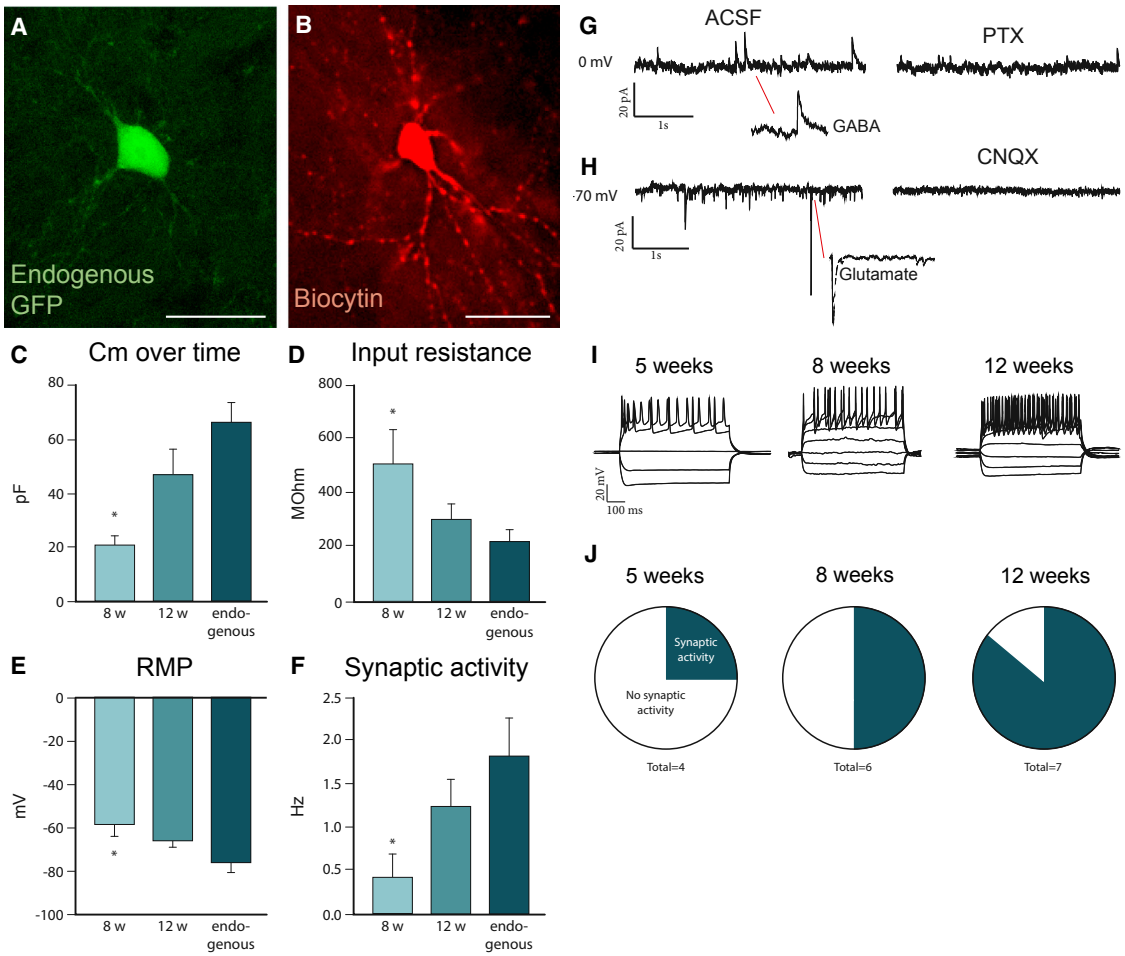

Figure 1. Reprogrammed Neurons Functionally Mature over Time

(A) Endogenous GFP expression can be detected in a reprogrammed neuron (unstained tissue) and was used to identify cells for recordings.

(B) Post-recorded biocytin-filled neuron shows mature neuronal morphology including dendritic spines.

(C–F) The reprogrammed neurons show maturation in membrane-intrinsic properties from 8 to 12 w.p.i., as shown for (C) membrane capacitance (Cm), (D) input resistance, (E) resting-membrane potential (RMP), and (F) frequency in spontaneous postsynaptic activity (for Cm, input resistance, and RMP, n = 6 [8 w.p.i.], n = 7 [12 w.p.i.], and n = 7 [endogenous]; for spontaneous postsynaptic activity, n = 4 [5 w.p.i.], n = 6 [8 w.p.i.], n = 7 [12 w.p.i.], and n = 5 [endogenous]).

(G and H) Traces showing (G) inhibitory (GABAergic) activity that was blocked with picrotoxin, a $GABA_A$ receptor antagonist and (H) excitatory activity that was blocked with CNQX, an AMPA receptor antagonist.

(I) Reprogrammed neurons show repetitive firing already at 5 w.p.i. and continue to show that at 8 and 12 w.p.i.

(J) The number of neurons with postsynaptic activity increases over time.

All data are presented as means ± SEM; *$p < 0.05$ in one-way ANOVA. Scale bars: (A and B), 25 μm. See also Figure S1.

For all these parameters, cells were not significantly different from endogenous cells by 12 w.p.i. (Figures 1C–1F).

Spontaneous inhibitory currents could be blocked with picrotoxin, and spontaneous excitatory currents could be blocked with CNQX (Figures 1G and 1H), indicating that reprogrammed neurons received synaptic input from both inhibitory and excitatory terminals, probably from nearby striatal neurons (GABAergic) and from more distal glutamatergic terminals (corticostriatal and thalamostriatal). While all cells but one (n = 17) showed repetitive firing from 5 w.p.i. (Figures 1I and S1C–S1F), few neurons at this time point showed postsynaptic activity. The proportion of neurons that displayed postsynaptic activity increased from 5 to 12 w.p.i. (Figures 1J and S1C–S1S).

ALN Reprogrammed Neurons in the Striatum Display Functional, Histological, and Molecular Properties Similar to Interneurons

A more detailed analysis revealed several distinct firing patterns. Only one of the patched cells showed firing

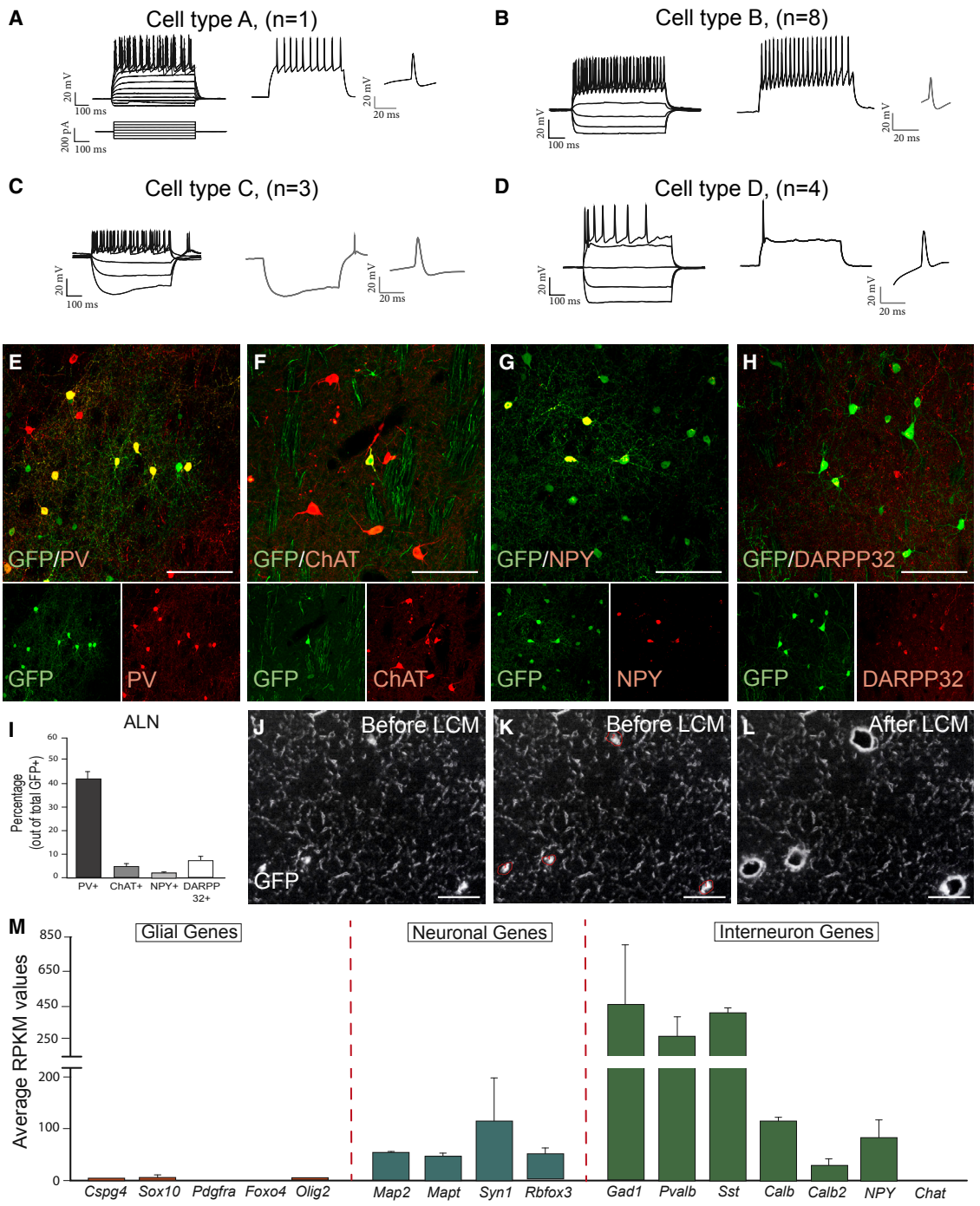

Figure 2. Phenotypic Identities of Reprogrammed Neurons

(A–D) The firing patterns were of four distinct types: (A) similar to endogenous medium-spiny neuron (1/16; cell type A); (B) similar to FSI (8/16, cell type B); (C) similar to low-threshold spiking cells with prominent sag (3/16, cell type C); (D) firing with large after-hyperpolarization (4/16, cell type D).

(E–H) Confocal images showing co-localization of GFP and the interneuron markers PV (E), ChAT (F), NPY (G), and projection neuron marker DARPP32 (H).

(I) Percentage of neurons expressing the markers from (E–H) shows that the majority of ALN-converted neurons are PV+ (n = 9 brains).

(legend continued on next page)

properties characteristic of striatal medium-spiny projection neurons (MSNs, cell type A in Figure 2A), while most cells showed a firing pattern similar to striatal IntNs (Figures 2B–2D) (Kawaguchi, 1993). Most cells displayed hyperpolarized resting membrane potential and similar firing frequency and input resistance as fast-spiking IntN (FSI) (Povysheva et al., 2013), with relatively short AP even though the AP duration and spike after-hyperpolarization were not yet in the range of their endogenous counterpart (Kawaguchi, 1993) (cell type B in Figure 2B and Table S1). Some cells showed other firing patterns reminiscent of long-lasting (LA) after-hyperpolarization or persistent and low-threshold spiking (PLTS) cells (cell type C and D, Figures 2C and 2D and Table S1). Immunohistochemical analysis at 12w.p.i. revealed the presence of markers common to IntNs such as PV (marker of FS cells), ChAT (marker of cholinergic, LA cells), NPY (marker of PLTS cells), or the striatal projection neuron marker DARPP32 (Figures 2E–2H). Quantifications showed that the majority (41.27% ± 2.99%) co-expressed PV, whereas less than 10% of the GFP+ cells were co-labeled with any of the other markers (Figure 2I). Thus, many of the IntN-specific markers that are not present at 6 w.p.i. (Torper et al., 2015) appear after additional maturation time *in vivo*.

To generate a transcriptional profile, we isolated ncGFP-expressing reprogrammed cells using laser capture microdissection (LCM) (Figures 2J–2L). Collected cells were pooled (n = 12–65 cells/sample) and prepared for polyA-based RNA sequencing (LCM-seq) (Nichterwitz et al., 2016). The sequencing data confirmed high expression levels of the reprogramming genes ALN (Figure S2E), downregulation of glial genes, and upregulation of pan-neuronal genes (Figure 2M). We also detected expression of IntN-linked genes (Figure 2M), confirming the histological and electrophysiological analysis.

DA Denervation or Reprogramming Region Does Not Affect Reprogramming Efficiency, Maturation, or Phenotype

We next tested if DA denervation that radically changes the striatal compartment and induces glia activation (Walsh et al., 2011) could affect reprogramming *in vivo*. *NG2*-Cre mice received a unilateral 6-OHDA toxin injection into the medial forebrain bundle (mfb lesion, n = 9), which produced a substantial loss of DA neurons in the SNc (Figures S3A and S3B) and subsequent loss of their projections to the dorsolateral striatum. Littermate control animals were left intact (n = 10).

Three weeks after lesions, animals were injected with ALN into the striatum and analyzed 12 w.p.i. GFP+ neurons were abundant in the lateral striatum and found in equal numbers in both intact and lesioned animals (Figures 3A, 3B, and S3C). TH+ cell bodies were found in the striatum of lesioned animals (Figure 3F) but not in intact controls (Figure 3E), which could be indicative of reprogramming into DA neurons under these conditions, as has been suggested in a recent study using similar DA conversion factors to reprogram resident mouse astrocytes (Rivetti di Val Cervo et al., 2017). However, none of the TH+ neurons were co-labeled with the GFP reporter (Figure 3F), suggesting that these were not *in vivo* reprogrammed neurons. Indeed, ectopic TH+ cell bodies were present in similar numbers in the striatum in control animals that were lesioned but not reprogrammed 15 weeks after lesion (Figures 3G and 3H). Like in the study by Rivetti di Val Cervo et al. (2017), most TH+ neurons in the control lesioned animals were negative for GABAergic IntN markers (Figures 3I and 3J) and positive for other DA markers, such as Nurr1 (Figure 3K), but only weakly expressing DAT (Figure 3L). Such ectopic striatal TH+ cell bodies have been found after lesion as reported in a number of studies (reviewed in Tepper and Koós, 2010), and we also confirmed their presence after 15 weeks in lesioned wild-type mice from a separate experiment (Figure S3K).

The reprogrammed neurons in both the intact and lesioned brains were analyzed using whole-cell patch clamp recordings. All neurons (n = 12) showed similar physiological properties with the ability to induce repetitive APs (Figures 3C and 3D) and also contained voltage-gated sodium and potassium currents (Figure S3D). Furthermore, the majority of cells (n = 9) displayed spontaneous postsynaptic activity (Figure S3E). The cells in the lesioned mice showed similar frequency in spontaneous activity as in intact mice (1.44 ± 0.36 Hz for intact, 1.52 ± 0.14 Hz for lesioned) (Figures 3C and 3D). None of the reprogrammed neurons recorded from displayed any DA-specific functional properties (Figure S3F).

We next tested if injecting the factors into the midbrain (homotopic environment for DA neurons) would influence the subtype toward DA identity. Analysis at 12 w.p.i. revealed the presence of GFP+ cells intermingled with endogenous nigral TH-expressing DA neurons (Figure 3M). None of the reprogrammed neurons co-expressed GFP and TH (Figures 3M–M″), even though a significant number of cells co-expressed GFP and the reprogramming factors ALN (Figures S3G–S3J).

(J–L) LCM was performed on nc-GFP-expressing cells: (J) before LCM; (K) before LCM; (L) after LCM.
(M) RNA-seq results, presented as average RPKM (reads per kilobase per million) values, show the downregulation of glial genes and upregulation of pan-neuronal genes and IntN-linked genes (n = 12–65 cells from n = 2–3 brains).
All data are presented as means ± SEM. Scale bars: (E–H), (J–L), 50 μm. See also Figure S2.

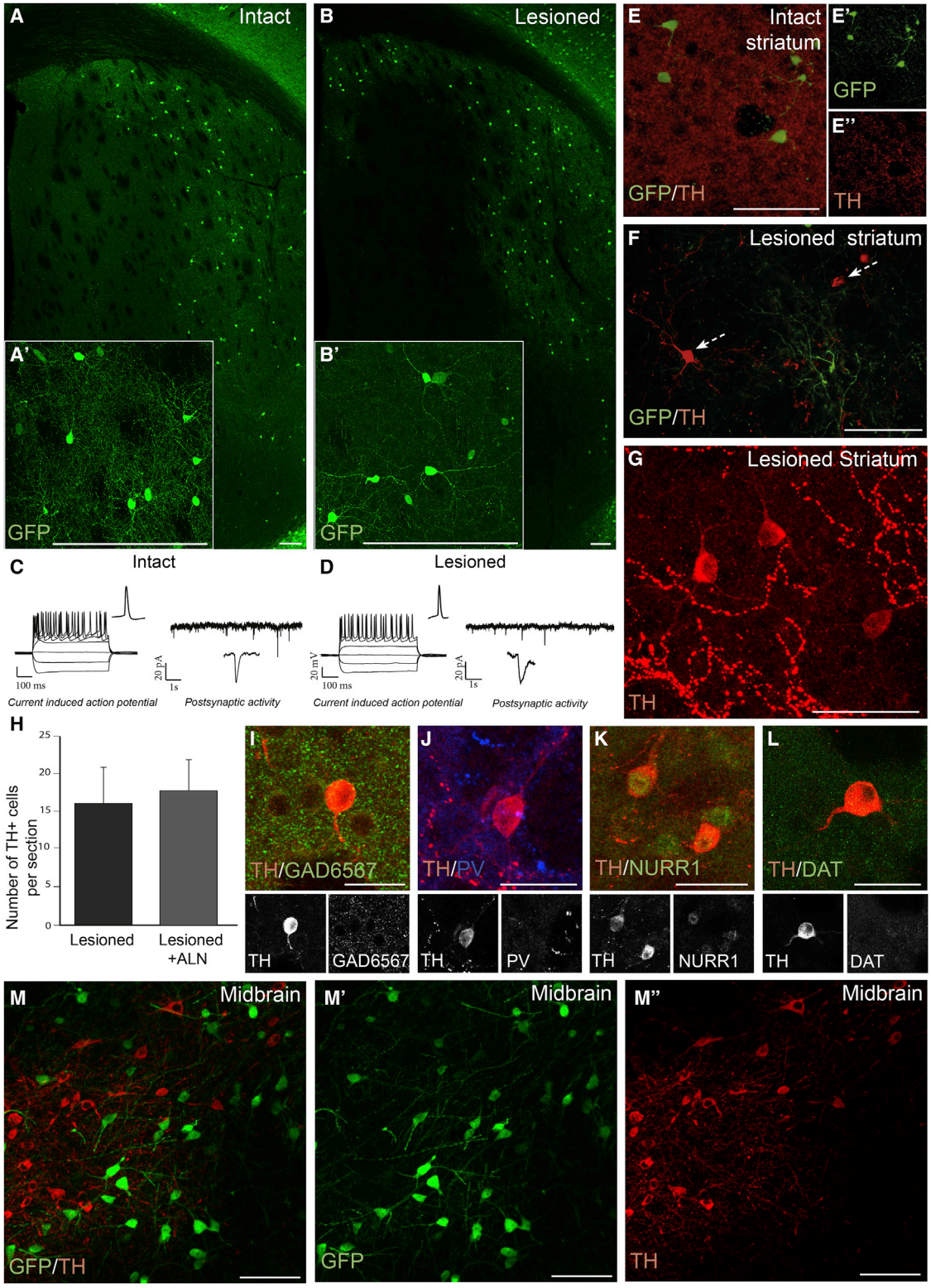

Figure 3. ***In Vivo*** **Reprogramming of Resident NG2 Glia in a DA-Denervated Striatum and in the Midbrain**

(A and B) Confocal images (stitched into a tile) of striatal sections showing GFP+ reprogrammed neurons that occur with similar efficiency (A and B) and morphology (A′ and B′) in the intact (A) and 6-OHDA lesioned (B) brain.

(legend continued on next page)

Overexpression of Different Gene Combinations in Striatal NG2 Glia

The appearance of IntNs after reprogramming using factors that give rise to DA neurons *in vitro* is intriguing and raises the question of how cell-fate conversion is controlled during *in vivo* conversion. We therefore next tested if different combinations of pro-neural (*Ascl1*, *Ngn2*, *NeuroD1*) and DA fate-specifying genes (*Lmx1a*, *Nurr1*, *FoxA2*, *En1*), could affect the phenotype of the converted neurons. Four different combinations of conversion factors, NgLN (*Neurogenin2*, *Lmx1a*, and *Nurr1*), ANgN (*Ascl1*, *Neurogenin2*, and *Nurr1*), NgN_{D1} (*Neurogenin2* and *NeuroD1*), and AFLE (*Ascl1*, *FoxA2*, *Lmx1a*, and *En1*), were injected either alone or together with the midbrain-specific chromatin remodeler *Smarca1* (Metzakopian et al., 2015) into the striatum of intact *NG2*-CRE mice (Figures 4A and 4B). GFP+ cells with complex neuronal morphology (Figures 4C″–4F″) could be observed in all groups. However, no co-expression of TH and GFP reporter could be detected (Figures 1C–1F and Figures 1C′–1F′). No GFP+ neurons were detected in control animals injected with the reporter vector alone (Figures 1G–1G″).

A more detailed phenotypic analysis of the reprogrammed neurons using the different factor combinations revealed that 9.03% to 27.01% of the reprogrammed cells expressed GAD65/67, while no VGlut1+ neurons were identified in any condition (data not shown). Similar to ALN, the largest proportion expressed the interneuron marker PV. ChAT+ and NPY+ neurons were found in lower percentages and CTIP2 was found in less than 10% of the reprogrammed neurons (Figures 4H and S4A–S4E).

DISCUSSION

In vivo reprogramming has emerged as a future possibility for brain repair. However, the phenotype of the reprogrammed cells obtained *in vitro* often differs from that obtained *in vivo* (Su et al., 2014). For example, several factors that convert astrocytes into neurons *in vitro* (Berninger et al., 2007; Heinrich et al., 2010) fail to do so *in vivo* (Grande et al., 2013). Our group has previously reported successful reprogramming of resident NG2 glial cells into neurons *in vivo*, using ALN. Despite the fact that these genes give rise to TH-expressing DA neurons when fibroblasts and astrocytes are reprogrammed *in vitro* (Addis et al., 2011; Caiazzo et al., 2011), no TH-expressing neurons were generated via *in vivo* reprogramming (Torper et al., 2015). Here, we reprogrammed NG2 glia in the 6-OHDA lesion mouse model, a condition that was also used in a study published during the revision of this manuscript, to reprogram mouse astrocytes using a slightly different combination of genes and miRNAs (Rivetti di Val Cervo et al., 2017). In both these studies, reprogramming was shown to be achievable in the DA-denervated striatum, which supports the use of *in vivo* reprogramming for brain repair. However, the interpretation of the finding that TH+ cells appear after reprogramming in the lesioned striatum (this study and the Rivetti di Val Cervo et al., 2017) is complicated as non-dopaminergic TH+ neurons appear spontaneously in response to the DA-denervating lesion (Tepper and Koós, 2010). We include a GFP reporter for identification of reprogrammed neurons and found that GFP did not co-label with TH. We conclude therefore that the neurons we observe are not TH+ DA neurons generated via reprogramming but rather striatal neurons that express TH in response to the lesion. In the Rivetti di Val Cervo et al (2017) study, the origin of the TH+ cells is unclear as no reporter was used, and no significant effect on DA-dependent behavior was observed. Thus, more work is needed in order to obtain functional DA neurons via *in vivo* reprogramming.

The functional properties of the reprogrammed neurons mature over time, and by 12 weeks the reprogrammed cells have phenotypic and functional properties of IntNs. The striatum is mainly composed of MSNs (95%) and, to a lesser extent, IntNs of different subtypes. Given the endogenous subtype distribution of striatal neurons, the selective conversion into neurons with properties of FSI expressing PV,

(C and D) Neurons in both conditions, (C) intact and (D) lesioned, showed repetitive current-induced action potentials (AP; traces on the left) and spontaneous postsynaptic events (traces on the right), in the absence of any drugs or stimulation.
(E) Reprogrammed neurons in the intact brain express GFP (E′), but not TH (E″).
(F) TH+ neurons were observed in the striatum after 6-OHDA mfb lesion, but these cells do not co-express GFP (arrows).
(G) Confocal image of abundant TH+ cells appearing in control animals (lesioned but no reprogramming factors).
(H) Quantification of the average number of TH+ cells found per section in control lesioned versus lesioned + reprograming factors groups (n = 6/group).
(I–L) Analysis of TH+ cells show that they do not express the striatal markers GAD65/67 (I) or PV (JK), but do express Nurr1 (K), and low levels of DAT (L).
(M–M″) *In vivo* reprogramming of resident NG2 glia in the midbrain results in endogenous TH+ cells (red) intermingled with GFP+ (green) reprogrammed neurons, with no overlap.
Data are presented as means ± SEM. Scale bars: (A–F) 100 μm; (A′ and B′) 100 μm; (G) 50 μm; (I–L) 25 μm; (M–M″) 50 μm. See also Figure S3.

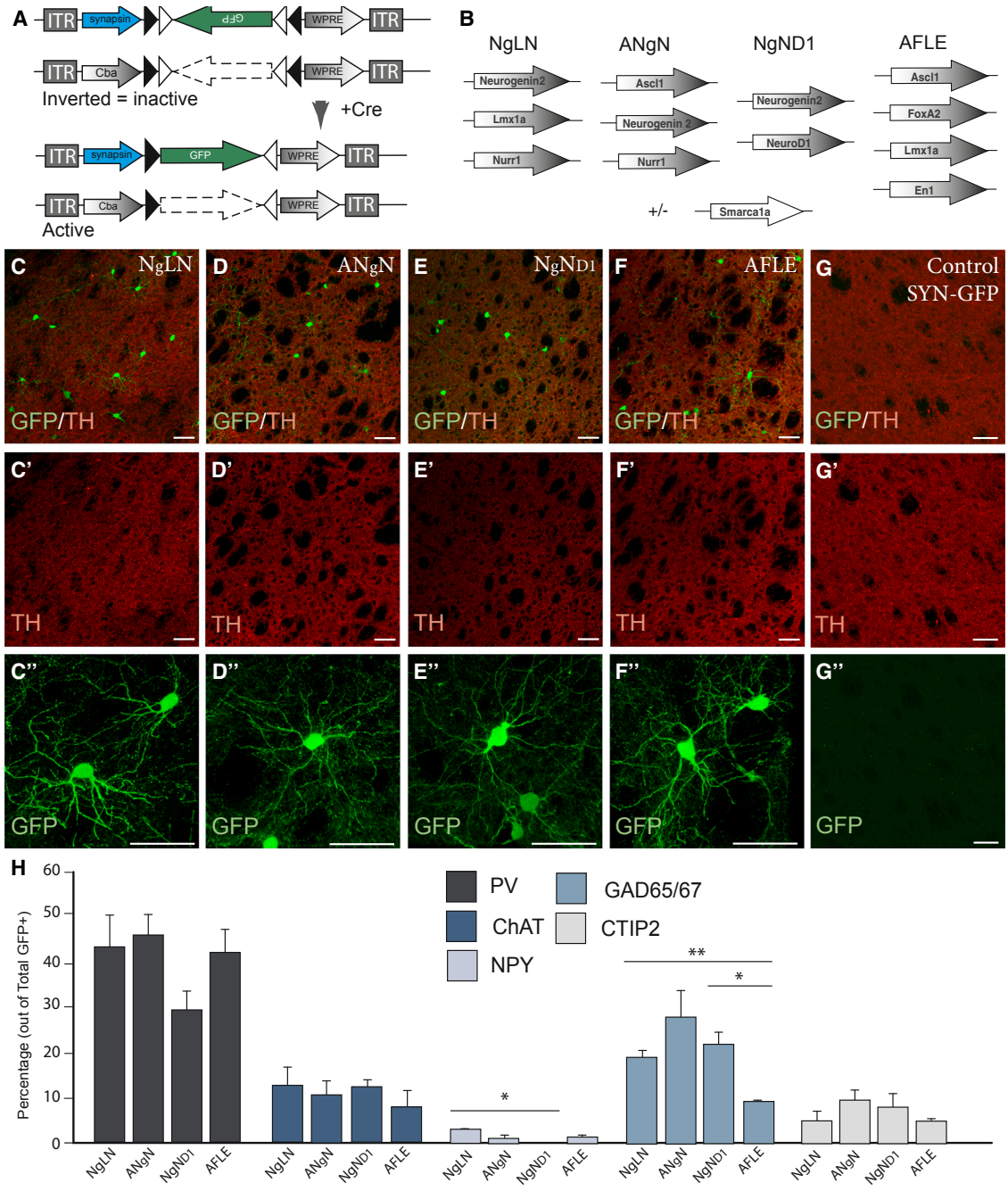

Figure 4. Different Gene Combinations Expressed in Striatal NG2 Glia Lead to Minor Differences in Neuronal Phenotype

(A) Schematics of AAV5 constructs used for *in vivo* reprogramming.

(B) Genes were grouped into four different combinations: NgLN, ANgN, NgN_{D1}, and AFLE. These groups of factors were used alone or in combination with *Smarca1a*.

(C–F) Confocal images showing the presence of GFP+ neurons 12 w.p.i. in the brains of *NG2*-Cre mice, when different combinations of genes were used for *in vivo* reprogramming: (C) NgLN, (D) ANgN, (E) NgN_{D1}, and (F) AFLE. (C″–F″) The reprogrammed neurons show a mature morphology but did not express TH.

(G–G″) In control animals where only *SYN*-GFP was injected in the brain of *NG2*-Cre mice, no GFP+ neurons were detected.

(H) Quantification of neurons reprogrammed with different factor combinations that express the markers PV, ChAT, NPY, GAD65/67, and CTIP2 shows that the majority of neurons obtained are PV-positive in all conditions (n = 3 brains/combination).

(legend continued on next page)

which normally accounts for less than 1% in the striatum, is noteworthy. This raises the question of how cell fate is influenced during *in vivo* conversion. We tested three different pro-neural genes (*Ascl1*, *Ngn2*, and *NeuroD1*), which have all been used previously for neural conversion (Grande et al., 2013; Guo et al., 2014; Liu et al., 2015), and found that independently of which neurogenic genes or fate determinants are used, the reprogrammed cells still were of an interneuron identity, and the different combinations had only minor impact on the subtype identity.

The presence of GABAergic neurons when Ngn2 was used for conversion may seem counterintuitive. However, during *in vivo* reprogramming, Ngn2 has previously been shown to drive both GABAergic and glutamatergic phenotypes (Grande et al., 2013; Gascon et al., 2016). This may be explained by differences in starting cell types that can have different transcriptional accessibility of target genes (Wapinski et al., 2013), or differences in the level of expression as high levels of Ngn2 drive glutamatergic differentiation in the developing forebrain but support GABAergic neuron formation when expressed at low levels (Parras et al., 2002).

GABAergic IntNs have previously been generated from resident glia, both in the latent state or after trauma such as stroke (Grealish et al., 2016). Our study shows the direct reprogramming of resident NG2 glia into neurons similar to FS, PV-containing IntNs, a subtype that plays a highly interesting role in striatal function. An initial deprivation of DA input in the striatum does create an imbalance in local circuits that involve IntNs (Martinez-Cerdeno et al., 2010), and GABAergic stimulation in the striatum could support and enhance the effects from intrastriatal DA transplants (Winkler et al., 1999). In line with this, intrastriatal transplantation of FSI precursors has even shown motor improvement in a rat Parkinson's disease (PD) model (Mallet et al., 2006). Moreover, striatal FSI dysfunction may underlie some forms of dystonia in PD (Gittis et al., 2011). This type of IntN has implications also in several diseases affecting the human striatum such as Tourette's syndrome, Huntington's disease, and paroxysmal dystonia (Reiner et al., 2013; Kalanithi et al., 2005; Gernert et al., 2000), which makes these neurons interesting from a therapeutic point of view (Spatazza et al., 2017).

EXPERIMENTAL PROCEDURES

Cloning and Viral Vector Production

Cre-inducible AAV5 vectors were created using a similar approach as in Torper et al. (2015).

Animals and Surgery

All experimental procedures were carried out under the European Union Directive (2010/63/EU) and approved by the ethical committee for the use of laboratory animals at Lund University and the Swedish Department of Agriculture (Jordbruksverket). Surgeries were performed under general anesthesia using 2% isoflurane mixed with air at a 2:1 ratio. For *in vivo* conversion experiments, 1 μL of vector mix (AAV5) was injected into the striatum of each animal at a rate of 0.4 μL/min with a diffusion time of 2 min.

Electrophysiology

Patch-clamp electrophysiology was performed on striatal brain slices from ALN-injected mice using same methods as in Torper et al. (2015).

RNA Sequencing of Nuclear GFP+ Cells Isolated by Laser Capture Microdissection

Mouse brains were dissected (n = 2–3 animals/group) after decapitation and snap frozen in 2-methylbutane (Sigma-Aldrich) on dry ice and stored at −80°C until further processed. Brains were sectioned in a cryostat at −20°C, and striatal sections with target GFP-positive cells placed onto PEN membrane glass slides (Zeiss) (three replicate slides per animal), which were kept at −20°C during the sectioning and subsequently stored at −80°C. Transcriptomic data were generated using LCM-seq (Nichterwitz et al., 2016).

For more detailed information, see Supplemental Information.

ACCESSION NUMBERS

The accession numbers for the gene sequences (the vectors available via Addgene) are as follows: *Ascl1*, RefSeq: NM_008553.4; *Lmx1a*, RefSeq: NM_033652.5; *Nurr1*, RefSeq: NM_013613.2; *Ngn2*, RefSeq: NM_009718.2; *NeuroD1*, RefSeq: NM_010894.2; *FoxA2*, RefSeq: NM_001291065.1; *En1*, RefSeq: NM_010133.2; *Smarca1*, RefSeq: NM_053123.4.

SUPPLEMENTAL INFORMATION

Supplemental Information includes Supplemental Experimental Procedures, four figures, and one table and can be found with this article online at http://dx.doi.org/10.1016/j.stemcr.2017.07.023.

AUTHOR CONTRIBUTIONS

M. Parmar, D.R.O., M. Pereira, J.A.B., and E.H. planned and structured the experiments. M. Pereira, S.S., M.B., J.A.B., and D.R.O. performed experiments. M. Pereira, D.R.O., and M. Parmar analyzed data and wrote the manuscript. All authors had input and gave final approval of the manuscript.

All data are presented as means ± SEM, and an unpaired t test was performed to evaluate differences between percentages of double-positive cells found among the four conditions (NgLN, ANgN, NgN_{D1}, AFLE); *p < 0.005 (p = 0.0018 for differences in NPY expression, and p = 0.0019 for differences in GAD65/67 expression); **p < 0.05 (p = 0.0081 for differences in GAD65/67 expression). Scale bars: all 25 μm. See also Figure S4.

ACKNOWLEDGMENTS

We thank Bengt Mattsson, Michael Sparrenius, Ulla Jarl, Elsy Ling, and Jenny Johansson for technical assistance, Angela Cencci Nilsson and Laura Andreoli for providing sections from lesioned wild-type mice, and Isak Wernehov for help with histology and analysis. The research leading to these results has received funding from the European Research Council under the European Union's Seventh Framework Program: FP/2007–2013 NeuroStemcellRepair (no. 602278) and ERC Grant Agreement no. 30971, the New York Stem Cell Foundation, the Swedish Research Council (grants to M.P. and E.H.), the Swedish Parkinson Foundation (M.P. and E.H.), and the Strategic Research Area at Lund University Multipark. D.R.O. was funded by the Parkinson Research Foundation, Svenska sällskapet för medicinsk forskning, Fysiografen, and Åhléns-stiftelsen in Sweden. M.B. and S.S. are funded via BrainMatTrain, European Union Horizon 2020 Program (H2020-MSCA-ITN-2015) under the Marie Skłodowska-Curie Initial Training Network and Grant Agreement No. 676408. M.P. is a New York Stem Cell Foundation - Robertson Investigator.

Received: March 9, 2017
Revised: July 28, 2017
Accepted: July 28, 2017
Published: August 24, 2017

REFERENCES

Addis, R.C., Hsu, F.C., Wright, R.L., Dichter, M.A., Coulter, D.A., and Gearhart, J.D. (2011). Efficient conversion of astrocytes to functional midbrain dopaminergic neurons using a single polycistronic vector. PLoS One *6*, e28719.

Berninger, B., Costa, M.R., Koch, U., Schroeder, T., Sutor, B., Grothe, B., and Gotz, M. (2007). Functional properties of neurons derived from in vitro reprogrammed postnatal astroglia. J. Neurosci. *27*, 8654–8664.

Caiazzo, M., Dell'Anno, M.T., Dvoretskova, E., Lazarevic, D., Taverna, S., Leo, D., Sotnikova, T.D., Menegon, A., Roncaglia, P., Colciago, G., et al. (2011). Direct generation of functional dopaminergic neurons from mouse and human fibroblasts. Nature *476*, 224–227.

Gascon, S., Murenu, E., Masserdotti, G., Ortega, F., Russo, G.L., Petrik, D., Deshpande, A., Heinrich, C., Karow, M., Robertson, S.P., et al. (2016). Identification and successful negotiation of a metabolic checkpoint in direct neuronal reprogramming. Cell Stem Cell *18*, 396–409.

Gernert, M., Hamann, M., Bennay, M., Loscher, W., and Richter, A. (2000). Deficit of striatal parvalbumin-reactive GABAergic interneurons and decreased basal ganglia output in a genetic rodent model of idiopathic paroxysmal dystonia. J. Neurosci. *20*, 7052–7058.

Gittis, A.H., Hang, G.B., LaDow, E.S., Shoenfeld, L.R., Atallah, B.V., Finkbeiner, S., and Kreitzer, A.C. (2011). Rapid target-specific remodeling of fast-spiking inhibitory circuits after loss of dopamine. Neuron *71*, 858–868.

Grande, A., Sumiyoshi, K., Lopez-Juarez, A., Howard, J., Sakthivel, B., Aronow, B., Campbell, K., and Nakafuku, M. (2013). Environmental impact on direct neuronal reprogramming in vivo in the adult brain. Nat. Commun. *4*, 2373.

Grealish, S., Drouin-Ouellet, J., and Parmar, M. (2016). Brain repair and reprogramming: the route to clinical translation. J. Intern. Med. *280*, 265–275.

Guo, Z., Zhang, L., Wu, Z., Chen, Y., Wang, F., and Chen, G. (2014). In vivo direct reprogramming of reactive glial cells into functional neurons after brain injury and in an Alzheimer's disease model. Cell Stem Cell *14*, 188–202.

Heinrich, C., Blum, R., Gascon, S., Masserdotti, G., Tripathi, P., Sanchez, R., Tiedt, S., Schroeder, T., Gotz, M., and Berninger, B. (2010). Directing astroglia from the cerebral cortex into subtype specific functional neurons. PLoS Biol. *8*, e1000373.

Kalanithi, P.S., Zheng, W., Kataoka, Y., DiFiglia, M., Grantz, H., Saper, C.B., Schwartz, M.L., Leckman, J.F., and Vaccarino, F.M. (2005). Altered parvalbumin-positive neuron distribution in basal ganglia of individuals with Tourette syndrome. Proc. Natl. Acad. Sci. USA *102*, 13307–13312.

Kawaguchi, Y. (1993). Physiological, morphological, and histochemical characterization of three classes of interneurons in rat neostriatum. J. Neurosci. *13*, 4908–4923.

Liu, Y., Miao, Q., Yuan, J., Han, S., Zhang, P., Li, S., Rao, Z., Zhao, W., Ye, Q., Geng, J., et al. (2015). Ascl1 converts dorsal midbrain astrocytes into functional neurons in vivo. J. Neurosci. *35*, 9336–9355.

Mallet, N., Ballion, B., Le Moine, C., and Gonon, F. (2006). Cortical inputs and GABA interneurons imbalance projection neurons in the striatum of parkinsonian rats. J. Neurosci. *26*, 3875–3884.

Martinez-Cerdeno, V., Noctor, S.C., Espinosa, A., Ariza, J., Parker, P., Orasji, S., Daadi, M.M., Bankiewicz, K., Alvarez-Buylla, A., and Kriegstein, A.R. (2010). Embryonic MGE precursor cells grafted into adult rat striatum integrate and ameliorate motor symptoms in 6-OHDA-lesioned rats. Cell Stem Cell *6*, 238–250.

Masserdotti, G., Gascon, S., and Gotz, M. (2016). Direct neuronal reprogramming: learning from and for development. Development *143*, 2494–2510.

Metzakopian, E., Bouhali, K., Alvarez-Saavedra, M., Whitsett, J.A., Picketts, D.J., and Ang, S.L. (2015). Genome-wide characterisation of Foxa1 binding sites reveals several mechanisms for regulating neuronal differentiation in midbrain dopamine cells. Development *142*, 1315–1324.

Nichterwitz, S., Chen, G., Aguila Benitez, J., Yilmaz, M., Storvall, H., Cao, M., Sandberg, R., Deng, Q., and Hedlund, E. (2016). Laser capture microscopy coupled with Smart-seq2 for precise spatial transcriptomic profiling. Nat. Commun *7*, 12139.

Parras, C.M., Schuurmans, C., Scardigli, R., Kim, J., Anderson, D.J., and Guillemot, F. (2002). Divergent functions of the proneural genes Mash1 and Ngn2 in the specification of neuronal subtype identity. Genes Dev. *16*, 324–338.

Povysheva, N.V., Zaitsev, A.V., Gonzalez-Burgos, G., and Lewis, D.A. (2013). Electrophysiological heterogeneity of fast-spiking interneurons: chandelier versus basket cells. PLoS One *8*, e70553.

Reiner, A., Shelby, E., Wang, H., Demarch, Z., Deng, Y., Guley, N.H., Hogg, V., Roxburgh, R., Tippett, L.J., Waldvogel, H.J., and Faull, R.L. (2013). Striatal parvalbuminergic neurons are lost in

Huntington's disease: implications for dystonia. Mov. Disord. *28*, 1691–1699.

Rivetti di Val Cervo, P., Romanov, R.A., Spigolon, G., Masini, D., Martin-Montanez, E., Toledo, E.M., La Manno, G., Feyder, M., Pifl, C., Ng, Y.H., et al. (2017). Induction of functional dopamine neurons from human astrocytes in vitro and mouse astrocytes in a Parkinson's disease model. Nat. Biotechnol. *35*, 444–452.

Spatazza, J., Mancia Leon, W.R., and Alvarez-Buylla, A. (2017). Transplantation of GABAergic interneurons for cell-based therapy. Prog. Brain Res. *231*, 57–85.

Su, Z., Niu, W., Liu, M.L., Zou, Y., and Zhang, C.L. (2014). In vivo conversion of astrocytes to neurons in the injured adult spinal cord. Nat. Commun. *5*, 3338.

Tepper, J.M., and Koós, T. (2010). GABAergic Interneurons of the Striatum. In Handbook of Behavioral Neuroscience, H. Steiner and K.Y. Tseng, eds. (Elsevier), pp. 157–178.

Torper, O., Ottosson, D.R., Pereira, M., Lau, S., Cardoso, T., Grealish, S., and Parmar, M. (2015). In vivo reprogramming of striatal ng2 glia into functional neurons that integrate into local host circuitry. Cell Rep. *12*, 474–481.

Vierbuchen, T., Ostermeier, A., Pang, Z.P., Kokubu, Y., Sudhof, T.C., and Wernig, M. (2010). Direct conversion of fibroblasts to functional neurons by defined factors. Nature *463*, 1035–1041.

Walsh, S., Finn, D.P., and Dowd, E. (2011). Time-course of nigrostriatal neurodegeneration and neuroinflammation in the 6-hydroxydopamine-induced axonal and terminal lesion models of Parkinson's disease in the rat. Neuroscience *175*, 251–261.

Wapinski, O.L., Vierbuchen, T., Qu, K., Lee, Q.Y., Chanda, S., Fuentes, D.R., Giresi, P.G., Ng, Y.H., Marro, S., Neff, N.F., et al. (2013). Hierarchical mechanisms for direct reprogramming of fibroblasts to neurons. Cell *155*, 621–635.

Winkler, C., Bentlage, C., Nikkhah, G., Samii, M., and Bjorklund, A. (1999). Intranigral transplants of GABA-rich striatal tissue induce behavioral recovery in the rat Parkinson model and promote the effects obtained by intrastriatal dopaminergic transplants. Exp. Neurol. *155*, 165–186.

Stem Cell Reports, Volume *9*

Supplemental Information

Direct Reprogramming of Resident NG2 Glia into Neurons with Properties of Fast-Spiking Parvalbumin-Containing Interneurons

Maria Pereira, Marcella Birtele, Shelby Shrigley, Julio Aguila Benitez, Eva Hedlund, Malin Parmar, and Daniella Rylander Ottosson

Figure S1
Related to Figure 1

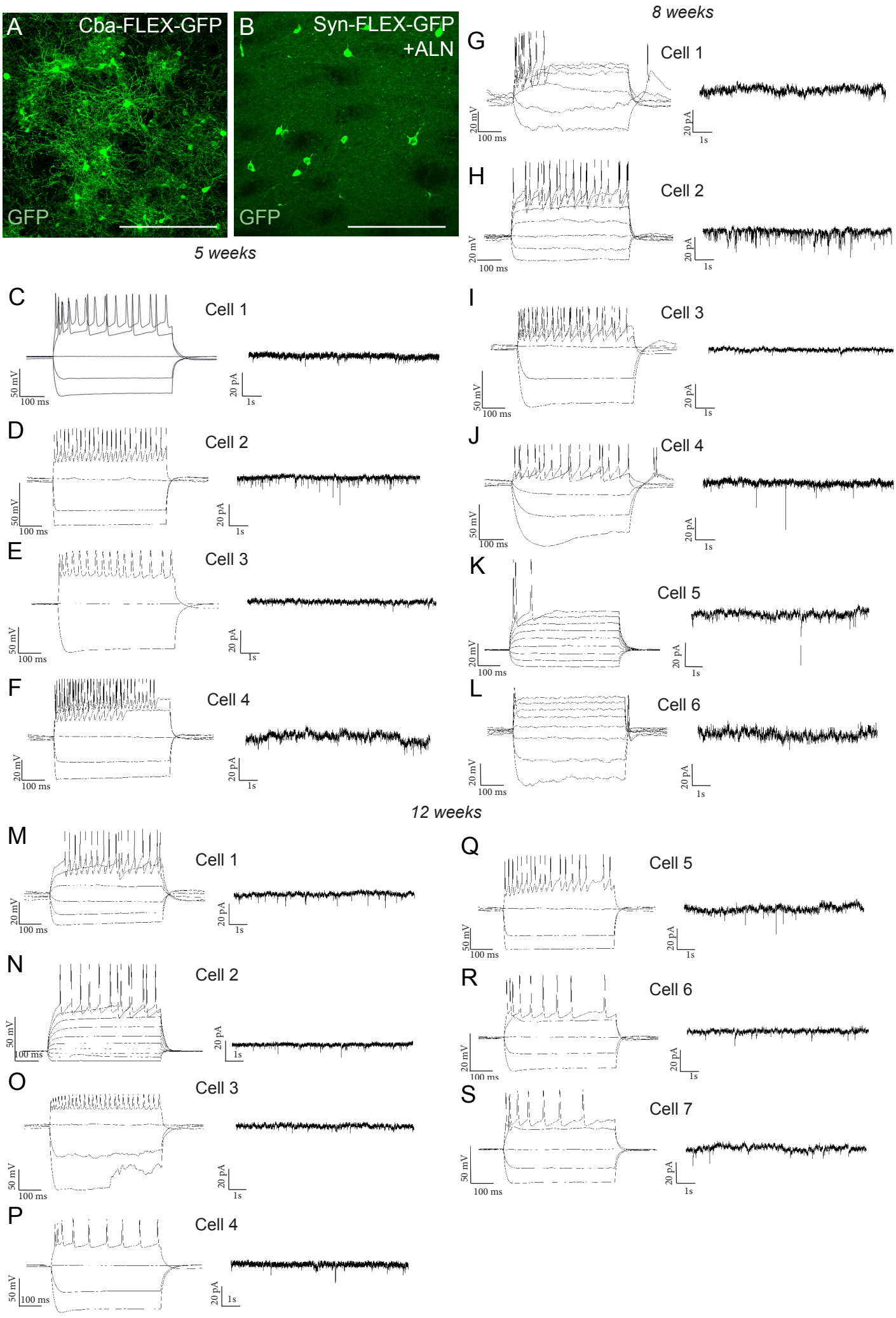

Figure S1 - Related to Figure 1

(A-B) Confocal images showing GFP+ cells in the striatum of mice injected either with (AAV5) Cba-FLEX-GFP, labelling NG2 glia (A), or (AAV5) SYN-FLEX-GFP, labelling neurons (B); (C-S) Individual traces from whole-cell recordings of reprogrammed neurons, 5 (C-F), 8 (G-L) and 12 (M-S) weeks post injection. Current-induced action potential (AP) and post-synaptic activity (current, in pA) of reprogrammed cells showed that the ability to induce repetitive AP preceded the ability to form post-synaptic contacts. After 5 weeks, only cell 2 (D) showed post-synaptic activity with event threshold of >5pA. (In cell 4 the baseline was too unstable to distinguish any synaptic events). All cells recorded showed repetitive AP after current injections. At 8 weeks, 3 cells out of 6 cells (cell 2,4 and 5 - H, J and K, respectively) showed synaptic events whereas 5 out of 6 showed repetitive spiking. At 12 weeks, 6 out of 7 cells showed postsynaptic activity (cell 3 did not show postsynaptic activity since events were not clear enough to be detectable for analysis). Scale bars A-B: 200 μm.

Figure S2
Related to Figure 2

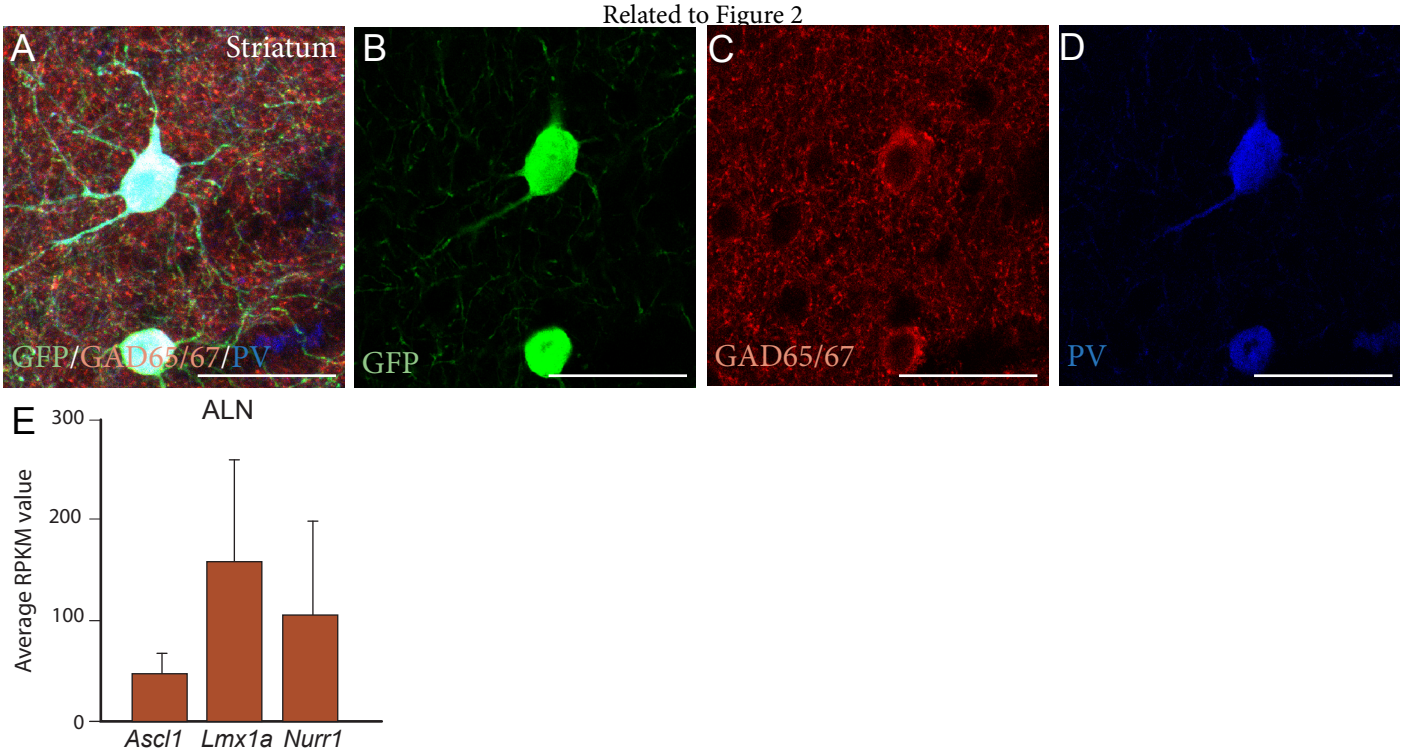

Figure S2 - Related to Figure 2
(A-D) Confocal images showing Parvalbumin-positive reprogrammed neurons (A, B and D) in the striatum of a mouse injected with SYN-GFP + ALN, expressing the striatal marker GAD65/67 (C); (E) The reprogramming factors ALN are detected at high levels in nuclear-GFP-expressing neurons, as demonstrated by RNAseq of neurons isolated by LCM (LCM-seq; n=12-65 cells collected from n=2-3 brains). Data presented as MEAN +/- SEM. Scale bars A-D: 25 µm.

Figure S3
Related to Figure 3

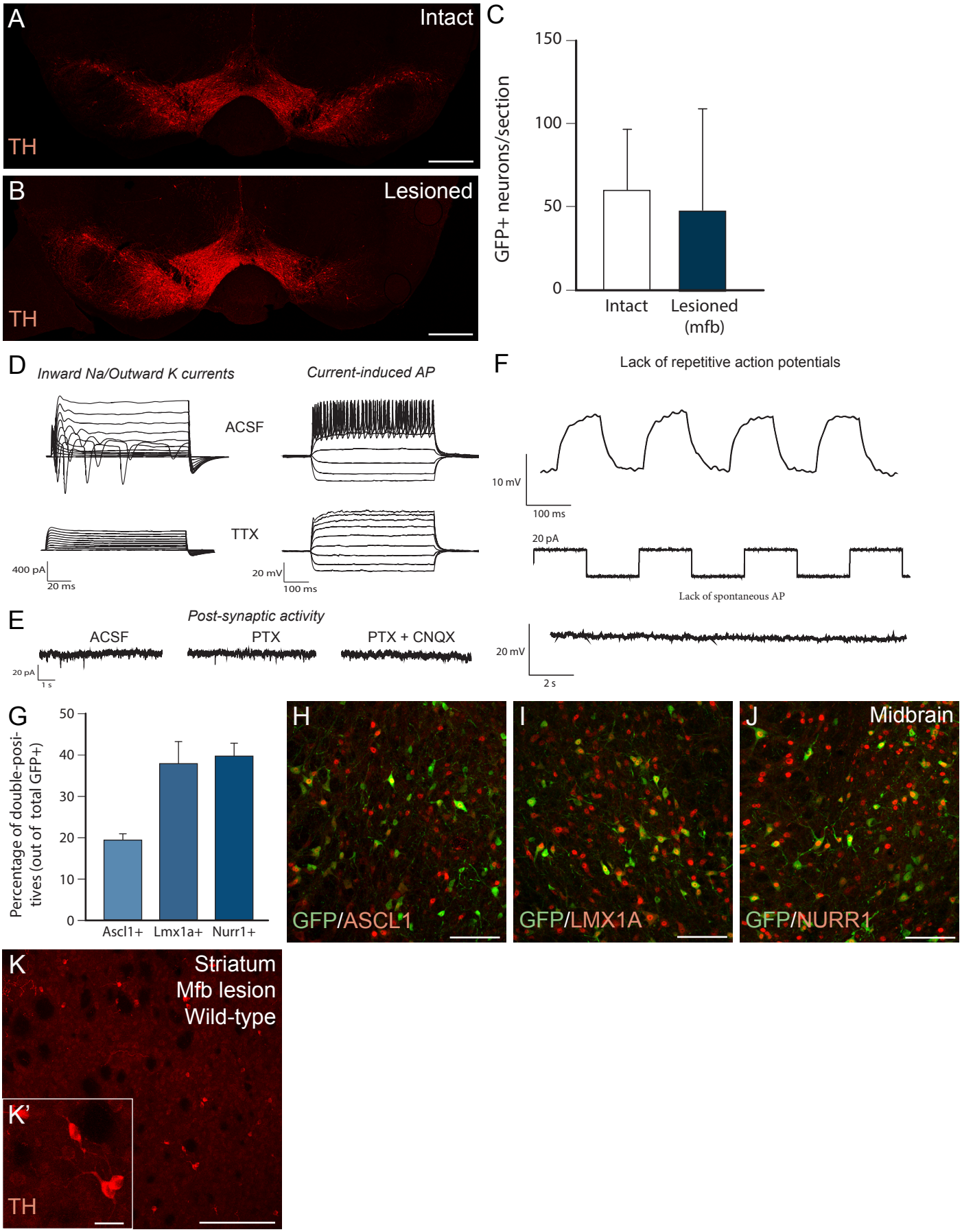

Fig. S3 – Related to Figure 3.
Tyrosine hydroxylase (TH) staining of the Subtantia Nigra showing a unilateral denervation on the right side, in a medial fore-brain bundle (mfb)-lesioned animal (B) but spared cell bodies in an intact animal (A); (C) Quantification of *SYN*-GFP+ neurons revealed no significant difference between intact and lesioned group (mean number of GFP+ cells/section was 60 ± 12,71 for intact and 48 ± 24,63 for lesioned striatum; P value = 0,6494; n=8 brains for intact and n=6 brains for lesioned); (D) Repro-grammed neurons expressed inward sodium and outward potassium currents at depolarizing steps, which could be blocked with the blocker of voltage-gated sodium-channel, tetrodotoxin (TTX) that also blocked AP; (E) Postsynaptic activity of reprogrammed neurons was seen with whole-cell patch clamp in both lesioned and intact brain, and this could be blocked with picrotoxin (PTX) and CNQX; (F) iNs showed no electrophysiological traits of DA phenotype such as repeated AP after small current injections or spontaneous AP; (G) Quantifications on sections from brains injected with ALN in the midbrain revealed the presence of overlap in percentages of cells expressing each one of the three markers (n=5 brains); (H, I, J) Confocal images showing the presence of *SYN*-GFP+ cells that co-label with Ascl1 (H), Lmx1a (I) or Nurr1 (J); (K) Confocal image shows TH+ cells in the the striatum of a wild-type lesioned mouse, which has not received any viral injection. Data presented as Mean+/-SEM. Scale bars A, B: 500 μm; H-J: 100 μm; K: 200 μm; K': 25 μm.

Figure S4
Related to Figure 4

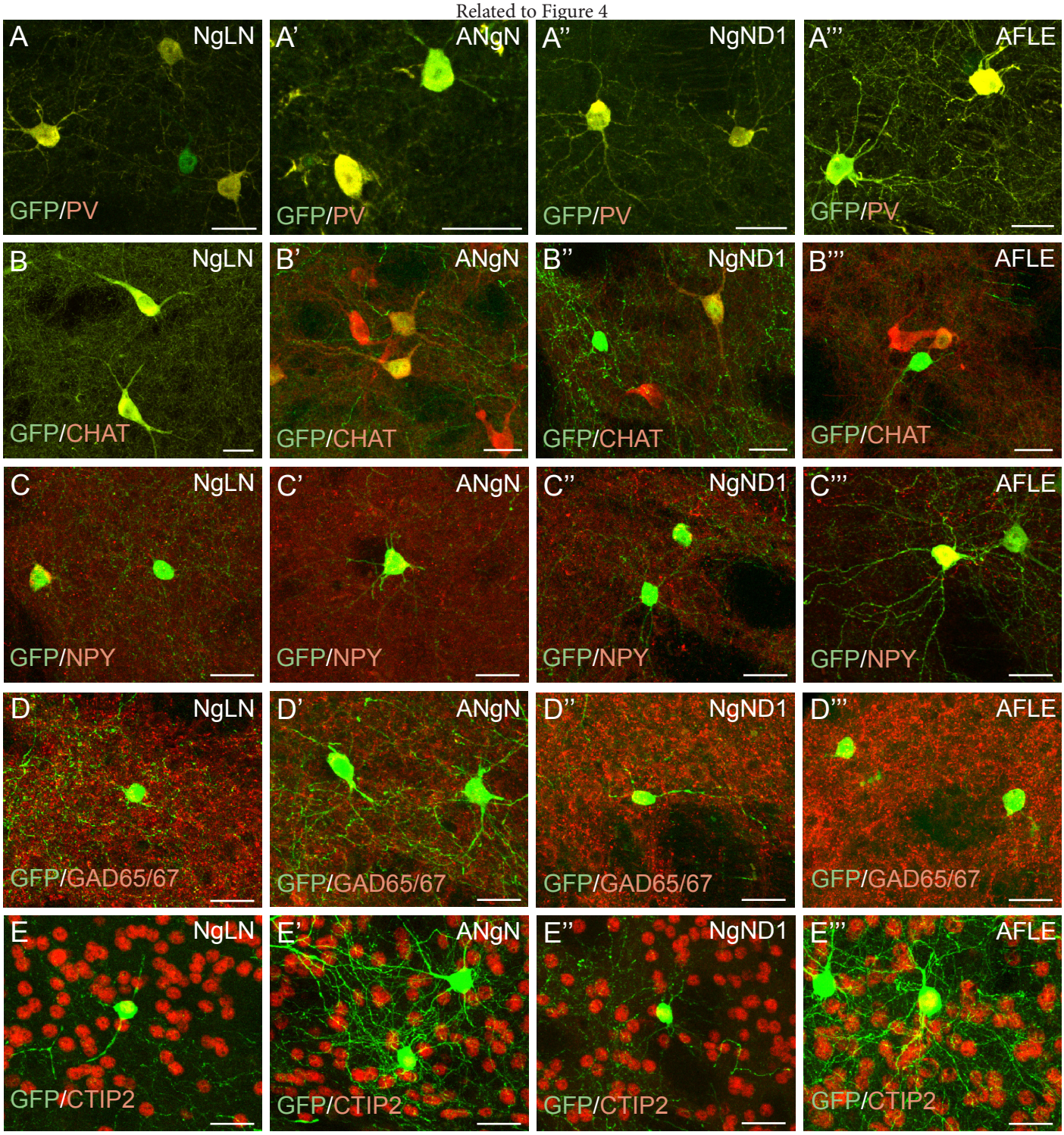

(A-E) Images show the presence of GFP+ cells in the striatum of NG2-CRE mice in which different factor combinations of genes were used for reprogramming. These GFP+ cells co-label with the markers PV (A, A', A'', A'''), CHAT (B, B', B'', B'''), NPY (C, C', C'', C'''), GAD65/67 (D, D', D'', D''') and CTIP2 (E, E', E'', E''') when the gene combinations NgLN, ANgN, NgND1 and AFLE are used. All scale bars: 25 μm.

Table S1: Electrophysiological parameters for the different types of reprogrammed neurons. Related to Figure 2.

Cell-type B (reminiscent of FSI) shows hyperpolarized resting RMP, similar firing frequency and input resistance as their endogenous counterpart but does not yet show all the properties of mature FSI (Povysheva et al 2013, Kawaguchi 1993). Cell type C in our manuscript has greater amplitude of afterhyperpolarization (AHP) after spike compared to the other groups, a greater input resistance and more depolarized RMP, that is similar to LA neurons (including cholinergic IntNs). It is still not in the exact range of endogenous counterpart (Kawaguchi 1993). Cell type D has a longer duration of AP compared to FS and long duration of afterhyperpolarization (time to peak of AHP in this table) that is similar to PLTS neurons (NPY-containing). Yet, for the other parameters, this cell type cannot be identified as a specific IntN subtype (n=1 for cell type A, n=8 for cell type B, n=3 for cell type C and n=4 for cell type D).

	Celltype A	Celltype B	Celltype C	Celltype D
RMP (mV)	-77 ± 0	-63,75 ± 2,82	-54 ± 4,34	-72 ± 2,45
Input resistance (MΩ)	110 ± 0	204 ± 27,6	730 ± 101,5	291 ± 70,34
Firering frequency (Hz)	28 ± 0	43,25 ± 4,09	28,67 ± 7,69	19 ± 2,08
AP duration, (ms, Spike width at half amplitude)	0,7 ± 0	0,61 ± 0,04	0,77 ± 0,12	1,05 ± 0,13
AHP amplitude (mV)	15 ± 0	10,5 ± 1,21	13 ± 1,73	7,02 ± 0,87
Time to peak of AHP (ms)	9,9 ± 0	6,15 ± 0,23	7,03 ± 0,55	12,25 ± 1,82
N of cells recorded	1	8	3	4

SUPPLEMENTAL EXPERIMENTAL PROCEDURES

Cloning and Viral vector production

Cre-inducible AAV5 vectors were created by inserting the cDNA for the genes of interest [1] in a reverse orientation flanked by two pairs of heterotypical, antiparallel LoxP (FLEX) sequences [2]. GFP was expressed under the control of a synapsin promoter, and *Smarca1a*, *Ascl1*, *Lmx1a*, *Nurr1*, *Neurogenin2*, *NeuroD1*, *FoxA2*, or *En1* were all regulated by a ubiquitously expressed chicken beta actin (cba) promoter. All constructs were sequenced prior to use. These Cre-inducible AAV5 vectors were produced according to [3] and each vector used individually or in mixture used at a 5% dilution in PBS.

Animals and surgery

All animals that were considered as dopamine (DA) lesioned in this study had a DA denervation in the substantia nigra pars compacta of >75% in comparison to the intact side (optical density analysis).

For *in vivo* reprogramming experiments in the striatum, the viral solution was injected at the following coordinates: AP = +1.0, ML = -2.0, DV = -2.7 relative to bregma, tooth bar = flat. For *in vivo* reprogramming experiments in the midbrain, the viral injections were performed at the coordinates: AP = -3.1, ML = -1.1 and DV = -4.0 relative to bregma, tooth bar = flat. For total 6-OHDA lesion experiments, 0.5 µl of 6-OHDA (3.2 µg/µl) was injected into the medial forebrain bundle (mfb) at the following coordinates: AP = -1.0, ML = -1.3 and DV = -4.75 relative to bregma, tooth bar = flat.

Immunohistochemisty

At the chosen experimental endpoints, animals were transcardially perfused with ice-cold 4% PFA, dissected and post-fixed for 12 hours in 4% PFA. In the following day, the brains were put in 25% sucrose for 12 hours, frozen and then cut on a microtome at 35µm of thickness in 8 series.

Sections were stained using standard protocols and the following antibodies: GFP (chicken, Abcam ab13970, 1:1000), TH (rabbit, Millipore ab152, 1:1000), parvalbumin (mouse, Sigma P3088, 1:2000), ChAT (goat, Chemicon ab144p, 1:200), NPY (rabbit, Immunostar 22940, 1:5000), Darpp32 (rabbit, Abcam ab40801, 1:1000), GAD65/67 (rabbit, Abcam ab49832, 1:1000), vGlut1 (rabbit, Synaptic systems 135303, 1:1000), Tbr1 (rabbit, Abcam ab31940, 1:300), CTIP2 (rat, Abcam ab18465, 1:1000), Calretinin (rabbit, Abcam ab702, 1:200). For fluorescent stainings, Alexa 488 (goat anti-chicken, Life Technologies A11039, 1:500), biotinylated antibodies (Jackson BA2001, BA1000, BA9500 and BA4001, 1:200) and Cy3 Streptavidin (Jackson 016-160-084, 1:200) were used as secondary antibodies.

RNA sequencing of nuclear GFP positive cells isolated by laser capture microdissection (LCM-seq)

For LCM, a Leica DM6000R/CTR6500 apparatus was used and cells captured with the Leica LMD7000 system under fluorescence light at 40X objective magnification. Before the session, slides were air dried for 10 minutes inside the microscope set up. To minimize contamination by surrounding tissue, only cells with clear nuclear GFP were collected using a close cutting outline. Laser power was kept at a minimum and light exposure reduced by closing the fluorescence shutter after drawing cell outlines. Relative humidity for all experiments was between 20 and 31 % and the temperature range was between 20 and 26 °C. An average of 33 cells were collected by gravity in each cap of 0.2ml PCR tubes. After the session, 5 µl lysis buffer (0.2% Triton X-100, with 2 U ml recombinant RNase inhibitor, Clontech) was added to each cap. Samples were spun down in a table top centrifuge (VWR) for 5-10 seconds, quickly labeled, sealed with parafilm (Pechiney Plastic Packaging) and snap frozen on dry ice. Samples were stored at -80 °C. Library preparation for sequencing was carried out using the Smart-seq2 protocol [4] with some modification as described in [5]). The quality and concentration of sequencing libraries was measured with an Agilent 2100 Bioanalyzer using the High Sensitvity DNA kit (Agilent). Equal amounts of the indexed libraries (a total of 15 samples) were pooled and sequenced in one lane. Samples were sequenced using an Illumina HiSeq2000 sequencer and reads were 43 bp in length. RNA-seq reads were mapped to the mouse reference genome mm10 (Ensembl version 78) by employing STAR (version 2.4.1) [6] with parameter -- outSAMstrandField intronMotif enabled. The number of uniquely mapped reads was calculated using featureCounts (version 1.4.6) [7] with default parameters. To quantify and normalize the expression of genes/ transcripts, Cufflinks and Cuffnorm (version 2.2.1) [8] was used with parameter - library-norm-method geometric. Quality control was conducted, with cutoffs of at least 1 million reads and 70% mapping ratio to the mm10 genome. All the RNA sequencing data generated in this study have been deposited in NCBI's Gene Expression Omnibus (GEO) and are accessible through GEO: GSE101091.

Electrophysiology

Mice were killed by an overdose of pentobarbital and brains were rapidly taken out and coronally cut on a vibratome at 275μm. Slices were transferred to a recording chamber and submerged in a continuously flowing artificial cerebrospinal fluid (ACSF) solution gassed with 95% O_2 and 5% CO_2 at 23°C. The composition of the ACSF was (in mM):126 NaCl, 2.5 KCl, 1.2 NaH_2PO_4-H_2O, 1.3 $MgCl_2$-$6H_2O$, and 2.4 $CaCl_2$-$6H_2O$, 22 NaHCO3, 10 glucose adjusted to pH 7.4.
Whole-cell patch-clamp recordings were made using Multi-clamp 700B (Molecular Devices), and signals were acquired at 10kHz using pClamp10 software and a data acquisition unit (Digidata 1440A, Molecular Devices). Input resistances and injected currents were monitored throughout the experiments. Borosilicate glass pipettes (3–7 MΩ) for patching were filled with the following intracellular solution (in mM): 122.5 potassium gluconate, 12.5 KCl, 0.2 EGTA, 10 Hepes, 2 MgATP, 0.3 Na_3GTP and 8 NaCl adjusted to pH 7.3 with KOH as in [9]. For biocytin filling, 1mg of biocytin salt was added to 1ml of internal solution. GFP-positive cells with neuronal morphology were patched and slowly filled with biocytin-containing internal solution for 20 min before slowly removing the electrode. Sections were fixed in 4 % paraformaldehyde overnight and stained with streptavidin-Cy3 (1: 600 in KPBS-T, 2h), for a morphological overview of reprogrammed cells.
Resting membrane potentials were monitored immediately after breaking-in in current-clamp mode. Thereafter, cells were kept at a membrane potential of -60mV to -80mV, and 500ms currents were injected from -20pA to +90pA with 10pA increments to induce action potentials (AP). Inward sodium and delayed rectifying potassium currents were measured in voltage clamp at depolarizing steps of 10mV. Spontaneous postsynaptic activity was recorded in voltage-clamp mode at -70mV. For distinguishing the inhibitory postsynaptic events the membrane potential was set to 0mV for inhibitory events and -70mV for excitatory. Off line analysis of spontaneous excitatory post-synaptic currents (EPSC) and inhibitory post-synaptic currents (IPSC) were performed using a threshold-event detection (>5pA) in Clampfit analysis program. CNQX, an AMPA antagonist and Picrotoxin (PTX), the $GABA_A$ receptor antagonist was added to the bath at the concentration of 20 and 50μM respectively (Tocris biosciences) to distinguish glutamatergic and GABAergic events.

Microscopy
Figures 3A, 3B, S3A and S3B are the result of the capture and stitching of individual images using a Leica TCS SP8 laser-scanning confocal microscope and corresponding software.
For non-confocal imaging, a Leica inverted Microscope (DFC360FX + DMI 6000B) was used.

Quantifications and statistical analysis
For quantification of GFP+ cells in intact and lesioned animals, neurons were counted in whole striatum and expressed as average of cells/section. Three striatal sections were counted per animal (n=8 animals for intact and n=6 animals for lesioned) (spanning from Bregma 1.7 to -0.26, as in [10]). Comparisons between the conditions lesioned and intact were made in Prism Graph-Pad using unpaired t-tests.
To calculate the conversion efficiency *in vivo*, the number of GFP+ cells was counted in sections from brains injected either with (AAV5)-Cba-FLEX-GFP (n=3) or (AAV5)-Syn-FLEX-GFP (n=9), and the number of neurons was compared with the number of NG2 glia cells found, and expressed as a percentage. A total of 3 sections per brain was analysed.
Quantification of different markers expressed in GFP+ neurons in the striatum, obtained with ALN (n=9) or with different combinations of factors (n=3 per combination) was done by counting the number of double-positive cells in relation to the total GFP+ cells found in two fields in the striatum. Two sections per animal were analysed. Differences between different conditions were analysed by using unpaired t-tests in Prism Graph-pad.
For quantifications of co-labelling of GFP/ASCL1, GFP/LMX1A and GFP/NURR1 in the midbrain region, two sections per animal (n=5) were analysed in each of three independent stainings. A rectangular region of interest was selected and cells within this area were counted. The mean number of double-positive cells per animal found in the three stainings was then compared.
For quantification of TH+ cells found in the striatum of lesioned animals, the number of TH+ cells per section was counted in Lesioned and Lesioned + ALN groups of animals (n=6 animals per group, n=6 sections per animal). All quantifications were performed in blind.
For membrane intrinsic properties (capacitance, input resistance, resting membrane potential and synaptic activity) one-way ANOVA was used with Bonferroni post-hoc test for multiple comparisons. N of cells compared for capacitance: n=6 (8w), n=7 (12w), n=7 (endogenous, i.e. MSNs and interneurons); for input resistance n=6 (8w), n=7 (12w), n=7 (endogenous); RMP n=6 (8w), n=7 (12w), n=7 (endogenous); for synaptic activity n=6 (8w), n=7 (12w), n=4 (5w), n=5 (endogenous).

SUPPLEMENTAL REFERENCES

1. Arenas, E., M. Denham, and J.C. Villaescusa, *How to make a midbrain dopaminergic neuron.* Development, 2015. **142**(11): p. 1918-36.
2. Atasoy, D., et al., *A FLEX switch targets Channelrhodopsin-2 to multiple cell types for imaging and long-range circuit mapping.* J Neurosci, 2008. **28**(28): p. 7025-30.
3. Zolotukhin, S., et al., *Recombinant adeno-associated virus purification using novel methods improves infectious titer and yield.* Gene Ther, 1999. **6**(6): p. 973-85.
4. Picelli, S., et al., *Full-length RNA-seq from single cells using Smart-seq2.* Nat Protoc, 2014. **9**(1): p. 171-81.
5. Nichterwitz, S., et al., *Laser capture microscopy coupled with Smart-seq2 for precise spatial transcriptomic profiling.* Nat Commun, 2016. **7**: p. 12139.
6. Dobin, A., et al., *STAR: ultrafast universal RNA-seq aligner.* Bioinformatics, 2013. **29**(1): p. 15-21.
7. Liao, Y., G.K. Smyth, and W. Shi, *featureCounts: an efficient general purpose program for assigning sequence reads to genomic features.* Bioinformatics, 2014. **30**(7): p. 923-30.
8. Trapnell, C., et al., *Transcript assembly and quantification by RNA-Seq reveals unannotated transcripts and isoform switching during cell differentiation.* Nat Biotechnol, 2010. **28**(5): p. 511-5.
9. Pfisterer, U., et al., *Direct conversion of human fibroblasts to dopaminergic neurons.* Proc Natl Acad Sci U S A, 2011. **108**(25): p. 10343-8.
10. Paxinos G, F.K.B.J., *The mouse brain in stereotaxic coordinates.* 2001, San Diego Accademic Press.